

# Geomagnetic Cutoff Calculations for the Interpretation of Low-rigidity Cosmic-ray Antiparticle Measurements

---

**Philip von Doetinchem\*, Bryan Yamashiro**

*Department of Physics and Astronomy, University of Hawaii at Manoa, Watanabe Hall,  
Honolulu, HI 96822, USA.*

*E-mail:* [philipvd@hawaii.edu](mailto:philipvd@hawaii.edu)

Low-rigidity cosmic rays and solar particles are strongly deflected by Earth's geomagnetic field and only particles above a certain geomagnetic cutoff rigidity are able to reach space-based or balloon-borne experiments. Geomagnetic cutoff calculations utilizing the PLANETOCOSMICS software with the IGRF geomagnetic field and the Tsyganenko magnetosphere models are discussed. These calculations focus on the time from 2011 to 2015 where the AMS-02 experiment on the International Space Station (ISS) was operational and are used to compare trajectories of cosmic-ray detectors on the ISS and balloon-borne experiments. A database approach was developed that allows very quick geomagnetic cutoff calculations, and thus an easy comparison of different trajectories. During the period under study time a particle-rich event that greatly perturbed the magnetic field strength on 7 March 2012 was observed and was studied in more detail from the geomagnetic cutoff perspective. All calculations put a special emphasis on antiparticles because precise measurement of their low-rigidity fluxes have the potential of revealing exotic sources like dark matter annihilations or primordial black holes. The findings underline that geomagnetic cutoff effects have to be treated as a function of particle charge, time, location, and direction.

*35th International Cosmic Ray Conference — ICRC2017  
10–20 July, 2017  
Bexco, Busan, Korea*

---

\*Speaker.

## 1. Introduction

A precise understanding of low-rigidity cosmic-ray antiprotons and antideuterons is important for the identification of dark matter [1]. One of the systematic uncertainties for data interpretation of low-rigidity data is the correction for effects introduced by the magnetic field in the vicinity of Earth, where the low-rigidity range is defined as 0.5–3.0 GV. Fig. 1 illustrates trajectories of antiprotons with different rigidities that were backtraced through Earth’s magnetosphere originating from the same location and with the same initial direction. The threshold rigidity at which particles are free to leave Earth’s magnetic environment is called the geomagnetic cutoff. As a consequence, a detailed understanding is especially important for the transition regions between trapped and free particles. A prominent example is the interpretation of the low-rigidity data from the AMS-02 cosmic-ray experiment [2], which is installed on the International Space Station (ISS) located at a  $51.7^\circ$  low Earth orbit. In this paper, the cosmic-ray flux is defined as the flux of particles penetrating from outside of the Earth’s magnetic environment, in contrast to the particles that are trapped within the geomagnetic field. To extend the measurement of the cosmic-ray fluxes to low rigidities, a careful understanding of the changing magnetic field over time is crucial.

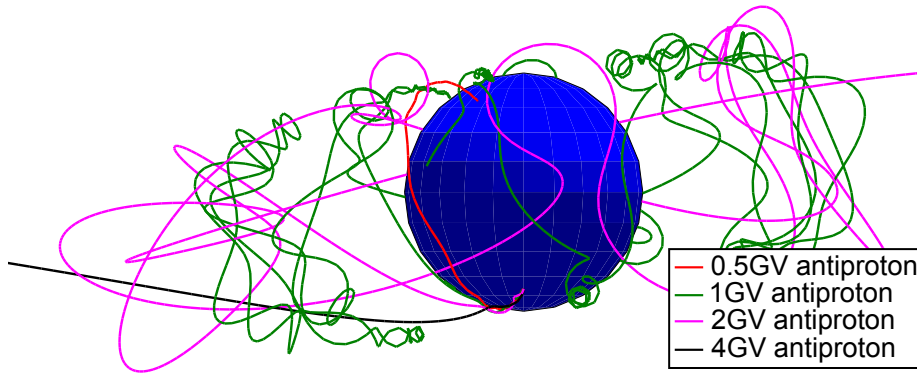


**Figure 1:** Reverse computation of antiproton trajectories starting at the same location ( $50^\circ\text{S}$ ,  $0^\circ\text{W}$ ) perpendicularly with respect to Earth’s surface for 19 May 2011 using the Tsyganenko 2004 model using PLANETOCOSMICS.

## 2. Magnetic Models

The following calculations utilize the geomagnetic field as described by the International Geomagnetic Reference Field (IGRF) [3]. In addition to the geomagnetic field produced by Earth’s rotating iron core, the magnetic vicinity of the Earth is altered by the influence of a constant flow of charged particles originating from the Sun, called the solar wind, which is described within the Tsyganenko 2004 (TSY04) model [4]. Key input parameters for this model are the tilt angle of the geomagnetic dipole, the disturbance storm time (Dst) index, and the dynamic solar wind pressure.

The measurement of cosmic rays is mostly carried out with detectors facing perpendicularly outwards from the Earth. As a result, the magnitude of the magnetic field component horizontal to Earth’s surface  $|B_h|$  has the strongest effect on perpendicularly incoming charged particles.

### 3. Geomagnetic Cutoff

#### 3.1 General Considerations

Geomagnetic deflection modulates the detectable charged cosmic-ray flux. As the geomagnetic field strength changes as a function of the geographical location and direction, the common approach for determining the origin of a charged particle is to backtrace it outside of Earth’s magnetosphere using the magnetic field models described in Sec. 2. Trajectories of particles at rigidities that perform several complex loops cannot escape the magnetosphere and are called “forbidden”. Trajectories of particles escaping Earth’s magnetosphere are called “allowed” trajectories. The rigidity corresponding to the last allowed trajectory for a certain geographic position and direction is called the “geomagnetic cutoff”. The following studies utilize the `Geant4`-based `PLANETOCOSMICS` [5] framework for backtracing charged particles, which is based on the established procedure described in [6]. For this purpose the latest IGRF-12 components [3] and the `TSY04` code were added to `PLANETOCOSMICS`. When mentioning the geomagnetic cutoff, the effective cutoff  $R_c$ , as defined in [6], is invoked. The effective cutoff is an average value, which takes into account the complex structure between regions of allowed and forbidden particle trajectories.

The geomagnetic cutoff depends on the geographic position. Operation of cosmic-ray experiments closer to the magnetic poles allow for measurements with significantly lower geomagnetic modulation for low-rigidity studies. Also some ISS orbits regularly exhibit exposure to the low-rigidity region of 1–3 GV, which will be discussed in more detail in Sec. 4.2. Fig. 2 also demonstrates, for a location of  $50^\circ\text{S}$ ,  $0^\circ\text{W}$ , that a dependence on both the particle inclination (zenith angle) and the azimuthal orientation is apparent. The low-rigidity region is shown in yellow, and this effect is explained by the structure of the local magnetic field. As a consequence, the charged particle detection rate does not only depend on location, but also on the direction. This caveat must be accounted for when interpreting low-rigidity cosmic-ray data.

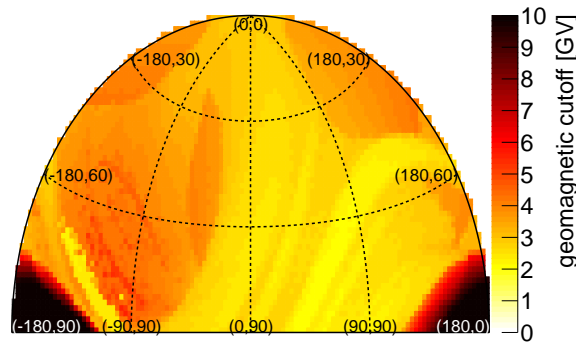


**Figure 2:** Geomagnetic cutoff calculations for antiprotons using the Tsyganenko 2004 model on 19 May 2011 at 400 km altitude (Aitoff projections). Cutoff values as a function of direction for a location of  $50^\circ\text{S}$ ,  $0^\circ\text{W}$ . The first value in the brackets denotes the azimuth and the second the zenith angle.  $(0,0)$  corresponds to perpendicular particle incident.

#### 3.2 Database

The driving idea behind building a geomagnetic cutoff database was to create a tool that promptly determines if a detected particle in a cosmic-ray detector was above cutoff without having

to execute the backtracing algorithm for each individual particle when analyzing a large-scale data set. The database approach is also an effective tool to quickly compare different flight trajectories of space-based and balloon-borne experiments. Systematic scans of geomagnetic cutoffs as a function of location in planetographic coordinates and direction for different times were executed on the University of Hawaii high performance cluster, corresponding to a total of more than 100 years of CPU time. The scanning ranges were chosen according to Tab. 1 and the altitude was chosen to be 400 km. A comparison between calculations at the typical ISS altitude of 400 km with a typical balloon flight altitude of 38 km for perpendicular particle incident for 19 May 2011 showed that the cutoff values agree within about 6%, and thus no altitude dependence between 38 km and 400 km will be considered. As the rigidity cutoff does not depend on the particle mass, the antiproton results can be directly transferred to antideuterons.

To calculate geomagnetic cutoff values for particles at positions and directions other than on the grid of Tab. 1, a weighted mean is calculated. Comparing cutoff calculations from event-by-event backtracings for antiprotons with isotropically chosen positions and directions for 19 May 2011 with cutoff values calculated from

the database shows an agreement within about 40%. This uncertainty has to be retained for the following sections. The key advantage of the database approach is that the interpolation essentially returns an instantaneous reply, while the calculation of one individually backtraced event can take up to about one minute on a state-of-the-art desktop computer. Many effects that are discussed in the following are larger than 40% and it is assumed that cutoff changes as a result of magnetospheric parameter variations are well reflected in the database approach.

**Table 1:** Geomagnetic cutoff range and step sizes.

angle	range [°]	step size [°]
latitude	-90 – 90	5
longitude	0 – 360	10
zenith	0 – 90	5
azimuth	0 – 360	10

### 3.3 Definition of Geomagnetic Efficiency

The geomagnetic cutoff efficiency  $\varepsilon$  as a function of rigidity is defined as the ratio of the measurement time of when particles of cosmic origin are within the acceptance of the detector and the total measurement time. If a particle is capable of reaching the detector location it is considered to be in the acceptance of the experiment if the zenith angle  $\alpha$  fulfills the requirement  $\cos \alpha > 0.6$ , which is a typical opening angle of cosmic-ray experiments.

## 4. The Geomagnetic Effect for Cosmic-ray Experiments at different Locations

As introduced above, the geomagnetic investigations in this study focus on the impact on low-rigidity cosmic-ray antiproton and antideuteron measurements. Two major instruments for this purpose are the operational AMS-02 detector on the ISS and the next-generation balloon experiment GAPS [7]. Therefore, this section discusses the geomagnetic differences between the ISS trajectory of AMS-02 and the projected Antarctic trajectory for GAPS. Furthermore, the geomagnetic cutoff efficiency for the first ULDB science flight of the Ultra Long Duration Balloon (ULDB) COSI 2016 flight from New Zealand [8] is presented.

#### 4.1 Cutoff for ISS and Balloon Flight Trajectories

The average geomagnetic cutoff efficiency over all ISS orbits is calculated by tracing the ISS for approximately 30,000 orbits. The calculation of the ISS position assumes an average altitude of 400 km and an inclination of  $\delta = 51.7^\circ$ . The ISS position is calculated every 10 s and for each of these instances a pair of direction angles is randomly chosen, following an isotropic distribution. The cutoff for this set of position and direction angles is computed from the database and used for the calculation of the average cutoff efficiency for the underlying database file. The calculation for (U)LDB trajectories follows the same idea, but uses the known balloon flight trajectories.

#### 4.2 Comparison

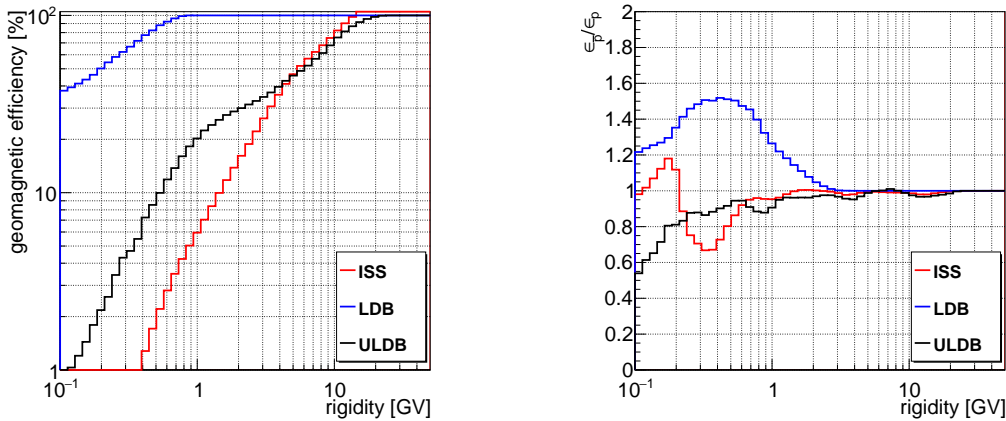


**Figure 3:** *Left)* Averaged geomagnetic efficiency for antiprotons at different flight trajectories, where the ISS values were averaged over cutoff simulations from 19 May 2011 to 6 October 2015 sampled every 100 days and the (U)LDB values were averaged over 5 December 2011, 8 January 2013, 12 February 2014, 10 December 2014 simulations, taking into account that balloon flights typically happen during the austral summer. *Right)* Averaged ratios of geomagnetic efficiencies of antiprotons and protons for the same time frames as in the top panel.

A comparison of the geomagnetic efficiencies as a function of rigidity for ISS and (U)LDB based experiments is shown in the left panel of Fig. 3. As expected, the closer a trajectory is to the magnetic poles, the higher the geomagnetic efficiency is for low-rigidity cosmic rays. For the ISS trajectory, on average about 50% of the cosmic-ray antiprotons at 7 GV reach the experiment while at about 1 GV only about 5% reach the ISS. Starting from about 20 GV the cutoff effect is negligible for the ISS trajectory. The first ULDB flight with a scientific payload spent a significant amount of time close to the equator and the geomagnetic efficiency for low rigidities was approximately 20% at 1 GV. In contrast, a typical LDB trajectory for a flight from McMurdo, Antarctica exposes a geomagnetic efficiency of nearly 100% at 1 GV. This highlights that the smallest systematic error for low-rigidity data related to the geomagnetic cutoff is achieved for Antarctic flights.

The right panel of Fig. 3 demonstrates the ratios of geomagnetic efficiencies for antiprotons with respect to protons. A uniform value of 1 over all rigidities would indicate that the geomagnetic cutoff efficiency is not charge dependent. However, due to the structure of the geomagnetic field, deviations from 1 are visible up to about 3 GV for all three trajectories. Furthermore, it is especially interesting to note that the ratios are heavily trajectory dependent. LDB flights from Antarctica are

especially well suited for antiproton measurements because antiprotons are less suppressed with respect to protons, resulting in a higher signal-to-noise ratio than on the ISS.

## 5. Time-dependent Geomagnetic Cutoff

### 5.1 Development from 2011 to 2015 for the ISS

As was pointed out by [9], solar magnetic disturbances influence the magnetic field in the vicinity of the Earth and can lead to considerable changes of the geomagnetic cutoff values as a function of time. Therefore, the geomagnetic changes were sampled in time steps of 100 days for the time interval between 19 May 2011 and 6 October 2015 (Fig. 4, left). The low-rigidity range exposes strong cutoff efficiency variations as a function of time and no trend is apparent for the 100 day sample rate. Sec. 5.2 discusses a much finer sampling for an extreme solar event, which does show a clear trend over a short amount of time.

Furthermore, the mean value of the horizontal magnetic field (averaged over a region from  $-20$  to  $20 R_{\oplus}$  in the  $x$ - $z$  slice at  $y = 0 \cdot R_{\oplus}$ ) was calculated and correlated with the geomagnetic efficiencies of different rigidities for the ISS trajectory (Fig. 4, right). The straight line fits indicate that the geomagnetic efficiencies scale linearly with the horizontal magnetic field strength, where a stronger field results in a larger geomagnetic efficiency for all rigidity steps. In the rigidity range of about 1 GV the cutoff efficiency is varying between 3–8% over time. This solar activity dependent effect clearly has to be taken into account when analyzing low-rigidity cosmic-ray data. The mean of the absolute horizontal magnetic field from 2011 to 2015 was 9.5 nT. Taking the straight line fits into account, this corresponds to mean geomagnetic efficiencies for the ISS of  $(4.8 \pm 0.3)\%$  at 1 GV and to  $(21.7 \pm 0.7)\%$  at 3 GV. Deviations from the mean values can be significant during strong solar activity. In this regard, the geomagnetic efficiency during March 2012 explicitly stands out and is discussed in more detail in Sec. 5.2.

### 5.2 Geomagnetic Cutoff During Solar Events

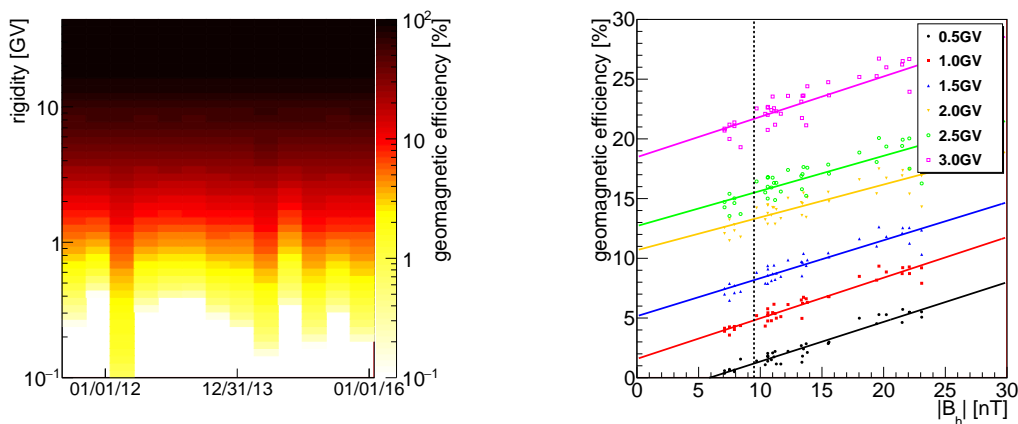


**Figure 4:** *Left*) Comparison of geomagnetic cutoff efficiencies for antiprotons reaching the ISS as a function of time. *Right*) Correlation of geomagnetic efficiencies for antiprotons reaching the ISS with the horizontal geomagnetic field component (ISS trajectory). The dashed perpendicular line indicates the mean horizontal magnetic field value from 2011 to 2015.

Periods of abnormal geomagnetic cutoff efficiencies were parsed to understand the effects of a perturbed magnetic field on a short-term timescale of a few days. As visible from the left panel of Fig. 4, March 2012 was characterized by a significantly different geomagnetic cutoff behavior compared to the other times under investigation. Therefore, the following analysis focuses on the extreme 7 March 2012 solar event, which was initiated by two solar flares, an X5.4 at 0:02 UT and an X1.3 flare at 1:05 UT, and followed by a coronal mass ejection consisting of large-scale plasma [10]. Consequently, the magnetic field strength dropped to a minimum Dst of  $-131$  nT on 9 March 2012, where the Dst does not deviate zero by more than 10 nT in a typical quiet period.

As already shown by [11], the effect of this large-scale solar event is also visible in the time evolution of the geomagnetic efficiency. The following goes a few steps further and studies the event with a higher sampling rate for antiprotons. The left panel of Fig. 5 shows the antiproton geomagnetic efficiencies for rigidities of 0.5–3.0 GV and the mean horizontal field as a function of time for the period of 8 to 10 March 2012 with sampling times of 1.5 h for the peak and 6 h for the quiet times. For better comparability, the geomagnetic efficiencies and magnetic field values were normalized to the average of the first and last time interval values for each curve. The dependence on rigidity is especially prominent from 0.5–1.5 GV. Rigidities from 2.0 GV and above show less deviation and illustrate that only lowest rigidities are greatly affected by geomagnetic storms. Nevertheless, even at 3 GV the change corresponds to about 20%. It is imperative to note the short timescale of the geomagnetic efficiency changes. Short-term modulations due to harsh solar activity are hidden by averages over longer time intervals, but the effects on low rigidity species are significant and must be considered. Rather than a long-term persisting elevation of geomagnetic efficiency, the efficiency levels return to the solar-quiet level within the same day of the maximum. This is also reflected in the change of the mean value of the horizontal magnetic field (averaged over a region from  $-20$  to  $20 R_{\oplus}$  in the  $x$ - $z$  slice at  $y = 0 \cdot R_{\oplus}$ ), which nearly happens on the same timescale as the geomagnetic efficiency. In absolute terms, the horizontal magnetic field  $|B_h|$  increased inside of the whole magnetosphere with respect to solar quiet periods by at least 30 nT and by more than 100 nT within a few Earth’s radii for the peak period.

The change in geomagnetic efficiency can also be illustrated spatially. The right panel of Fig. 5 shows the geographic locations of the ISS for different times during the solar event with antiproton cutoff values of less than 2.5 GV. The calculation followed the same principle as described in Sec. 4 and does not only represent locations with perpendicular zenith angles. This figure illustrates that cosmic-ray detectors on the ISS have sensitivity to antiprotons below 2.5 GV for some part of the extreme latitude regions, but never between approximately  $-35^{\circ}$  and  $35^{\circ}$ . The allowed areas for the solar event under study are the largest between 6:00 UT and 15:00 UT while the 0:00 UT and 18:00 UT areas expose “forbidden channels” that appear to run directly through the allowed areas. These changes are again short timescale effects that happened within hours and are correlated with the geomagnetic efficiency values shown in the right panel of Fig. 5.

## 6. Conclusion

Extensive geomagnetic cutoff calculations as a function of time were carried out using the PLANETOCOSMICS software. These took into account the changes in the magnetosphere as described within the data-driven Tsyganenko 2004 model. In conclusion, the geomagnetic correction

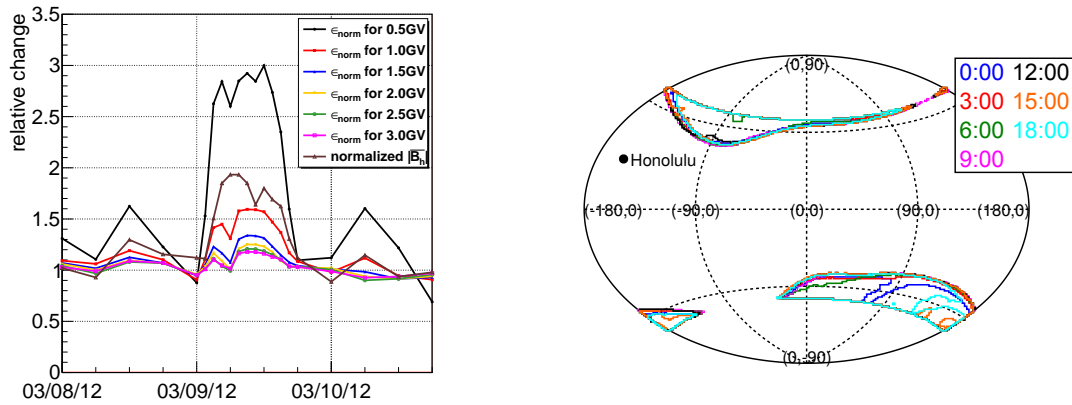


**Figure 5:** *Left*) Normalized geomagnetic efficiency ( $\epsilon_{\text{norm}}$ ) for the ISS trajectory and mean horizontal magnetic field  $|B_H|$  over time for the 7 March 2012 event. *Right*) The enclosed areas indicate regions for different times on 9 March 2012 where the geomagnetic cutoff for antiprotons is below 2.5 GV and the ISS spends at least 0.5% of its averaged orbit (Aitoff projection).

in the analysis of data from cosmic-ray experiments has to be treated as time-dependent. This variability can happen on timescales as short as a few hours for extreme solar event cases.

## Acknowledgments

The work of PvD was supported by the National Science Foundation under Award No. 1551980. The work of BY was supported by the Hawaii Space Grant Consortium. The support and advanced computing resources from University of Hawaii Information Technology Services- Cyberinfrastructure are gratefully acknowledged. The authors would like to thank Alan Chiu for providing the COSI Ultra Long Duration Balloon flight trajectory.

## References

- [1] T. Aramaki et al., *Astroparticle Physics* 59, 12 (2014), T. Aramaki et al., *Physics Reports* 618, 1 (2016).
- [2] R. Battiston, *Nuclear Instruments and Methods in Physics Research A*, 588, 227 (2008).
- [3] E. Thébault et al., *Earth, Planets and Space* 67(1), 1 (2015).
- [4] N. A. Tsyganenko and M. I. Sitnov, *Journal of Geophysical Research: Space Physics*, 110(A3) (2005).
- [5] L. Desorgher et al., 36th COSPAR Scientific Assembly 36, 2361 (2006).
- [6] D. J. Cooke et al., *D. J., Il Nuovo Cimento C*, 14(3), 213 (1991).
- [7] C. J. Hailey, *New Journal of Physics* 11(10), 105, 022+ (2009).
- [8] J.-L. Chiu et al., *Nuclear Instruments and Methods in Physics Research A* 784, 359 (2015).
- [9] D. Smart and M. Shea, 34th COSPAR Scientific Assembly 34, 2424 (2002), M. Shea and D. Smart (2006), *Advances in Space Research* 38(2), 209, (2006).
- [10] D. Lingri et al., *Solar Physics* 291(3), 1025 (2016).
- [11] D. Grandi et al., *PoSICRC2015* 116 (2016).